CFD VALIDATION OF FILM FLOWS BY NOVEL HIGH-SPEED LIQUID FILM SENSOR WITH HIGH SPATIAL RESOLUTION

M. Damsohn*, H.-M. Prasser

Laboratory of Nuclear Energy Systems,
Institute of Energy Technology, ETH Zurich,
Switzerland

Abstract

A sensor is presented that allows high-speed measurements of two-phase film flows. The sensor consists of electrodes flush to the wall that measure the electrical conductance in the liquid film. This novel sensor has a time resolution of 10 kHz and 64x16 measuring points with a spatial resolution of 3.12 mm^2 and a maximum film thickness range of 0.8 mm. The shape of the sensor electrodes is optimized by calculating the potential field of the liquid film. Dynamic measurements of co-current air-water flow in a horizontal channel with an obstacle have been conducted. The high time and spatial resolution allows a wave analysis over a wide range of wavelengths and wave velocities. Statistical analysis methods are presented to characterize the flow pattern e.g. for comparison with CFD simulations.

1 INTRODUCTION

A lot of research has been done in the area of film and annular two phase flow over more than 50 years. A considerable amount of work was dedicated to droplet entrainment and deposition, wave properties and flow patterns. For these studies a variety of methods have been developed to measure the liquid film thickness dynamics. Among the experiments mainly four different principles are used:

- Extraction
- Photons
- Ultrasound
- Electricity

Extraction
The extraction method is used to investigate the total entrainment and deposition rate between the liquid film on the pipe wall and a droplet laden core flow. Usually the experimental setup consists of two porous circumferential rings flush to the pipe wall through which the liquid film is extracted. The first ring extracts the film to dry the wall. After a desired distance the second ring extracts the film that builds up between the two extraction rings by the deposition of the droplets (e.g. Assad, 1998).

Photons
Among the optical methods photography, absorption, fluorescence, diffraction and x-ray tomography are used, of which only the first three give sufficient spatial and time resolution to describe dynamic liquid films. Optical methods are generally non-intrusive and are able to deliver a high spatial resolution.
Especially interesting because of the high spatial resolution is the laser induced fluorescence. Alekseenko (2007) recently presented the use of a 2-D LIF for the investigation of the wave evolution on liquid falling films with a spatial resolution of 0.1 mm. The time resolution is below 50 Hz.

Ultrasound
Two-phase film flow ultrasonic film thickness measurements e.g. were carried out by Kamei (1998), who measured the film thickness circumferentially with 40 positions on a simulated nuclear fuel rod with a time resolution of 250 Hz. The time of flight measurement was done with a 10 MHz source with 10 kHz emission frequency and a rotating "mirror" in the fuel rod. This method is non-intrusive, but has its limitations in the measurement of small film thicknesses as well as combining high time resolution with high spatial resolution.

Electricity
Electrical methods have been widely applied for many years in the area of air-water annular pipe flow. They are mostly based on the relationship between conductance and liquid film thickness between a pair of electrodes, in most cases flush to the wall. Therefore the liquid must be electrically conductive. For nonconductive liquids, there is the possibility of making use of the relationship between the electrical capacity and film thickness (Takahama,1980). Most of these methods are used for the research on two-phase annular flow (e.g. Sekoguchi, 1998).

Compared to the other methods, electrical methods have generally the highest time resolution. If the electrodes are flush to the wall, this method is non-intrusive but limited for research on thick liquid films. It lies in the nature of this method that compared to optical methods the spatial resolution is limited, as will be explained later in this work.

Purpose of this work
Our own efforts were directed towards two-dimensional arrays of electrodes that are scanned by a fast multi-channel conductance measuring system. This method was developed by Prasser (1998) for wire-mesh sensors and proposed to be used for the signal acquisition of an array of 32x10 measuring points consisting of electrodes flush to the wall. Such a sensor with 5 kHz time resolution was developed by Belt (2007) and used for film thickness studies of annular flow in a vertical pipe.
The present work aims at a perfection of this method in order to increase spatial and time resolution as well as sensitivity and measuring range of the film thickness for different areas of research.

2 SENSOR CHARACTERISTICS

2.1 Sensor Design

The basic idea for the fast acquisition of time sequences of two-dimensional film thickness distributions is an array of electrode pairs mounted flush to the wall. When a voltage pulse is supplied to the first electrode (transmitter electrode) of each pair, a current flows to the second electrode (receiver electrode), that is put to zero potential. The current is depending on the thickness of an electrically conducting liquid film covering both electrodes. As shown in Figure 1 the two-dimensional array is arranged in such a way that the transmitting electrodes are connected in one direction (transmitter lines), while the receiver electrodes are coupled perpendicular to this direction (receiver lines). The voltage pulses are supplied to the transmitter lines in successive order. During the excitation of each transmitter line, all currents arriving at the receiver lines are sampled in parallel. After the excitation of the last transmitter electrode, a complete matrix of primary measuring values is recorded. These values represent the conductance distribution in the liquid film on the sensor surface, which is the measure of the film thickness.

The signal acquisition method used for this sensor is equivalent to the one of the wire-mesh sensors, which is described in detail in Prasser (1998). A special feature of the wire-mesh electronic circuitry is the low impedance of transmitter driver and receiver pre-amplifier cascades, which guarantees that the potential at all non-activated transmitter electrodes and all receiver electrodes remains very close

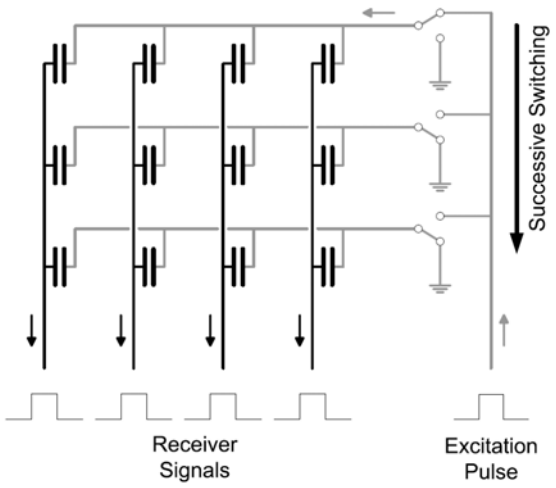

Fig.1: Circuitry of the sensor matrix

to ground potential. This is an important feature to suppress cross-talk to far located receiver electrodes, as discussed in Prasser (1998).

It lies in the nature of electrodes mounted flush to the wall, that there is a non-linear relationship between measured conductance and film thickness. Due to the fact that the potential field has a higher concentration in the region close to the wall, the sensor becomes less sensitive with growing film thickness. For thick films a saturation of the measured conductance is reached, which limits the range of the film thickness measurement. The dependence between film thickness and conductance (sensor characteristic) is influenced by the geometry of the electrodes.

This led us to the point of modeling the potential field in the liquid film on top of the sensor for optimizing shape and size of the transmitting, receiving and grounded electrodes to achieve the following characteristics:

- quasi linear sensor characteristic for low film thicknesses
- high measurement depth
- minimization of signal delocalization (“cross-talk”)
- high spatial resolution

In the course of this optimization, technological limits of the PCB-production had to be considered as boundary conditions.

The calculation of the sensor characteristic is done by solving the three-dimensional potential equation within the liquid film on top of the sensor electrode system. The calculation domain is a parallelepiped with the bottom face representing the electrode geometry of the sensor. Independent from the individual electrode shape, which is subject to the discussed optimization, the sensor is a two-dimensional matrix of electrode pairs, between which the conductance measurement takes place. The domain is discretized into a three-dimensional matrix of finite elements of cubical shape. The steady-state potential equation is solved with the method of finite differences. The calculation of the potential field is carried out for various film thicknesses. The electric currents at the different conducting areas are obtained from the potential field gradient integrated over the surface of the respective electrode. Symmetry relations were used to define a cutout of the sensor geometry that reflects the potential field of the whole sensor with a sufficient accuracy. In this way calculation costs can be kept bearable.

The results are based on a discretization step width of 50 µm of the calculation domain. The electrode surface is discretized with about 120 x 30 finite elements. The highest number of volume elements (~150000) is reached at maximum film thickness of about 40 elements. The number of elements slightly depends on the studied geometry.

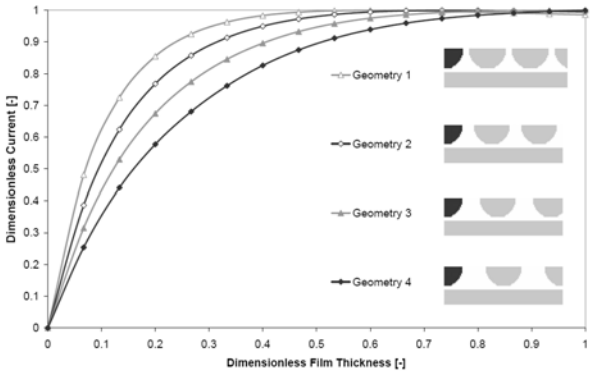

Fig. 2: Sensor characteristic with varying distance between the electrodes

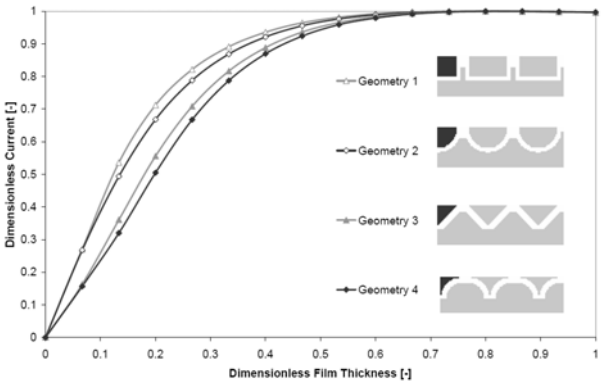

Fig. 4: Sensor characteristic with varying shape of the electrodes

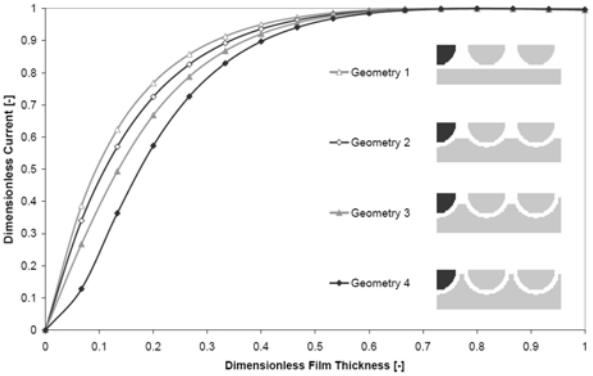

Fig. 3: Sensor characteristic with varying ground area between electrodes

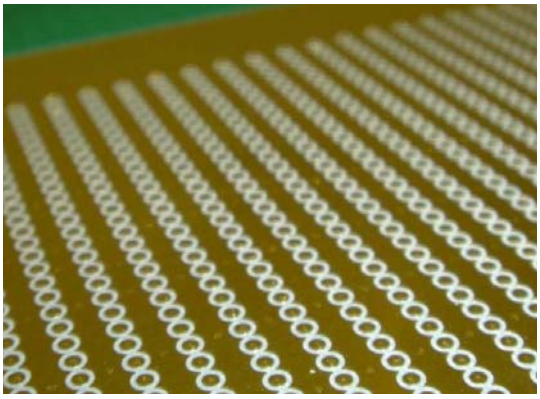

Fig. 5: Picture of sensor surface

Certain principles become obvious from the optimization of the sensor geometry:

1. With increasing distance between the electrodes the saturation film thickness increases (Figure 2). A limitation is set by the desired spatial resolution within the sensor plane, which decreases with increasing electrode distance.
2. The shape of the ground influences the shape of the sensor characteristics. Generally it can be stated that the further the ground reaches into the insulating gap between the electrodes, the higher is the saturation film thickness. On the other hand these grounded “noses” may cause a concave characteristic for small film thicknesses (Figure 3). There is a technological limitation from the production of PCBs that require a minimum radius of conducting surfaces.
3. By narrowing the shape of the electrodes towards each other the saturation film thickness increases (Figure 4). This effect is mainly caused by the increase of the specific ground area between the electrodes. The main limitation in this case is the production of the PCB. Because the electrodes need to be contacted to a lower layer of the multilayer PCB, the electrode shape has to contain at least a circular area of the minimum cross section of the layer connection, which corresponds to a diameter of 1 mm for the applied PCB technology. Further there is a minimum radius required for the production of the electrode surface.

Derived from these principles the electrode geometry of the developed sensor consists of circular electrodes with a medium sized “ground nose” (Figure 5). This leads to an almost linear sensor characteristic for low film thicknesses and a fairly high saturation film thickness in relation to the spatial resolution.

The sensor presented in this work consists of electrodes arranged in 64 lines with 16 pairs of alternating transmitter and receiver electrodes. The electrodes are spaced 1560 microns apart from

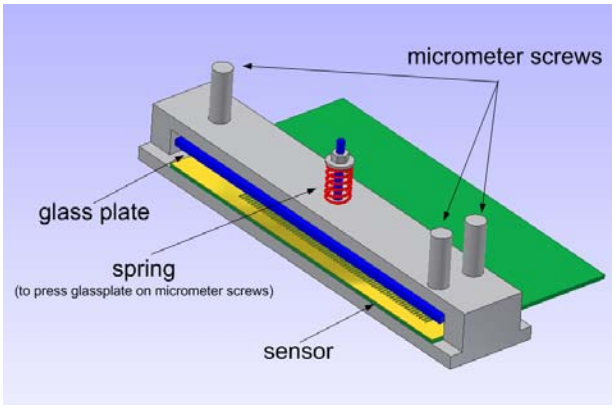

Fig. 6: Experimental setup for sensor calibration

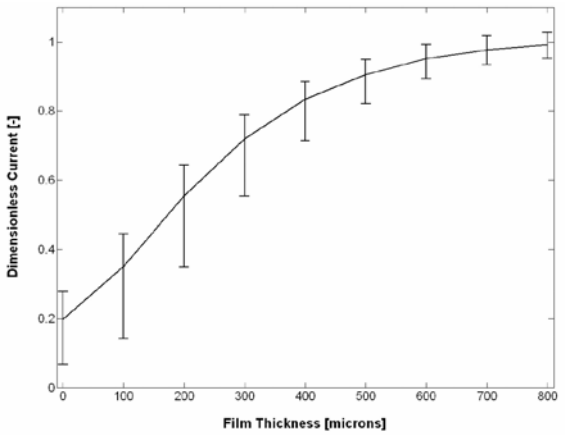

Fig. 7: Calibration result of the averaged sensor characteristic. Error bars indicate the deviation of the characteristic over the sensor matrix.

each other which leads to a spatial resolution of 3120 microns. The wire mesh electronic is able to sample the whole sensor matrix (frame) of 64x16 measuring points in 0.1 ms.
The "cross-talk" is the electrical current flowing between transmitting and far situated receiving electrodes. This means, that the measuring volume is increased in such a way, that the data is "smeared out" between the measuring points. This undesired effect received special attention during the electrode optimization. For the present sensor the calculations show, that the error caused by cross-talk is at most 0.5% of the value measured by the electrodes close to the transmitter electrode.

2.2 Calibration

For the calibration degassed water was filled in a basin in which the sensor was pressed on a stiff aluminum plate. Above the sensor a glass plate was moved vertically up and down by three micrometer screws in nine equidistant steps from 0 to 800 microns (Figure 6). Further the saturation current of the sensor was measured with a film thickness higher than 1200 microns, which is used to normalize the calibration. The calibration was done for eleven different water conductivities ranging from demineralized water (0.001 mS/m) to tap water (0.3 mS/m).
The shape of the sensor characteristic received by this method (Figure 7) is close to the calculated characteristic of the potential field calculation. The offset at zero film thickness originates from a very thin water film that remains between the glass plate and the sensor.
The calibration results show a standard deviation over time of less than 3%, which is mainly a result of electrical noise. There is however a significant scattering of the sensor characteristic over the sensor matrix, which is mainly a result of the electronics. This scattering makes a calibration for each measuring point necessary.
As mentioned before the calibration was carried out for different water conductivities. Except for water with low conductivity the shape of the sensor characteristic does not change significantly with the water conductivity. The deviation for low conductive water is caused by the higher amplification in the electronics.
The results of this calibration are used for the calculation of the film thickness from the primary measuring data of dynamic liquid films. A 4^{th} grade polynomial is fitted to the nine points (inversed from Figure 7) for each measuring point in the calibration by a curve fitting algorithm. Because the shape of the polynomial does not change with the water conductivity, it can be scaled by the ratio of the saturation currents of the calibration and the measurement. This way the calibration can be used for a wide range of water conductivities.
The accuracy of the calibration was evaluated on data from a repeated calibration experiment. This evaluation shows that for film thicknesses up to 500 microns an absolute accuracy of 20 microns is

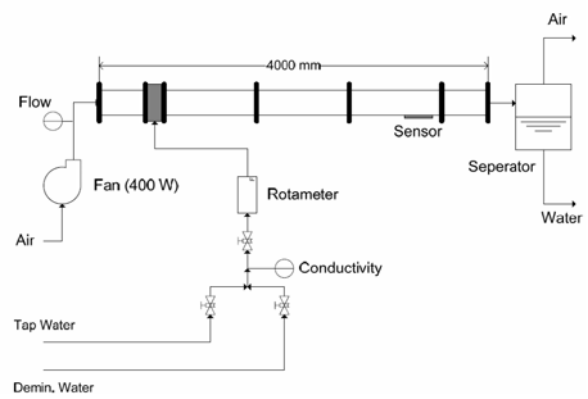

Fig. 8: Experimental setup for dynamic film thickness measurements

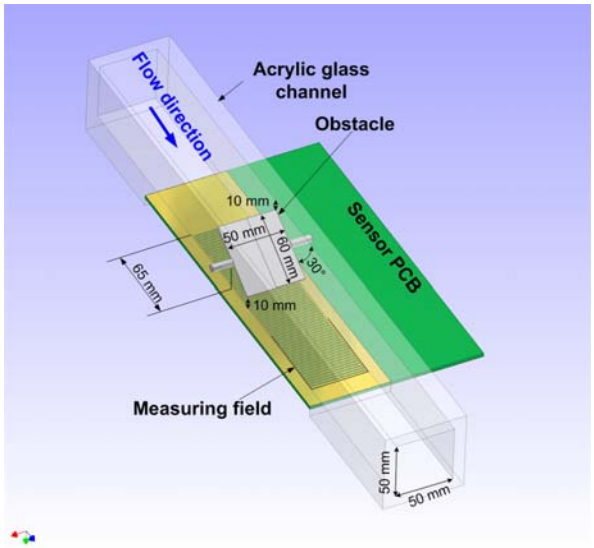

Fig. 9: Testsection

achieved for static films with the applied calibration method. For film thicknesses up to 800 microns the accuracy is reduced to 50 microns due to the reduced sensitivity of the sensor close to saturation.

3 EXPERIMENTS

3.1 Setup

The experimental setup for the dynamic film thickness measurements consists of a fan blowing through a test section, which is a cross sectional square (50x50mm) acrylic glass channel (Figure 8). The water injection is 500 mm behind the inlet of the acrylic glass channel. The sensor is mounted flush to the inside wall 2700 mm downstream of the water injection. A special module injects tap water directly as film on the bottom wall. Behind the sensor the acrylic glass channel continues for approximately 500 mm before entering a tank for air-water-separation. Because the sensor is sensitive to changes of water conductivity, it is checked throughout the measurement. The flow rate of the water is measured by a rotameter, whereas the flow rate of the air is measured with an Accutube® based on the principle of a Pitot tube.

For the investigation presented in this work a plate (60x50x2mm) is mounted vertically centered above the sensor with an angle of 30°. The tips of the plate are 10 mm from the bottom (respectively top) wall, so that the obstacle is not in contact with the liquid film (Figure 9). Hence the air flow is accelerated below the obstacle influencing the liquid film flow. The flow geometry has been chosen because it generates a changing shear stress at the gas liquid interface due to the acceleration of the gaseous phase, which is a typical challenge for the modeling of functional fuel rod spacers equipped with vanes.

3.2 Experimental Conditions

All measurements where carried out under adiabatic conditions at a temperature of 20°C and an ambient pressure of 980 hPa. Tap water was used for the liquid film with a conductivity of 0.3 mS/m. The fluid velocities were varied with 10, 15, 20 m/s for the superficial gas velocity and 0.003, 0.005, 0.007 m/s for the superficial liquid velocity. Experiments were conducted with all velocity combinations.

In this paper only the experiment with 10 m/s superficial gas velocity and 0.003 m/s liquid velocity is presented because these conditions have the lowest computational cost in future CFD simulations.

4 RESULTS AND DISCUSSION

Three methods are presented to distinguish the liquid film properties qualitatively and quantitatively, which might be applied for the comparison of experimental data and future CFD simulations:

- appropriate visualization for qualitative comparison
- mean film thickness
- wave propagation velocity

These methods have been applied to the experimental data to check their capability of characterizing and analyzing the flow.

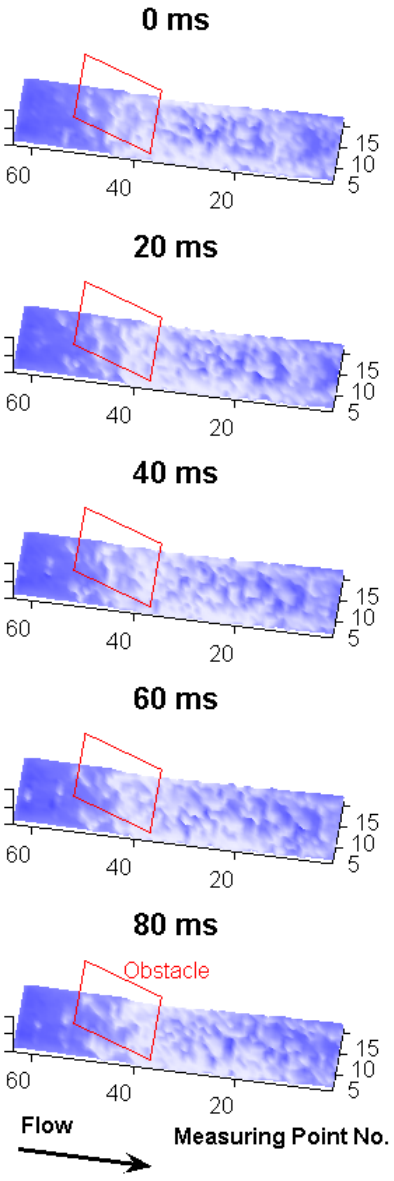

Fig. 10: 3D bird view of measured data

4.1 Visualization

The 3D-bird view (Figure 10) of the measured data shows following basic flow phenomena:

- the water film accumulates upstream of the obstacle (measuring point 64 to 52)
- the water film is thin under the end tip of the obstacle (measuring point 40 to 35)
- waves are generated downstream of the obstacle (measuring point 35 to 1)

For a qualitative comparison of wave velocities and wave length in longitudinal direction, one longitudinal line from the center of the sensor is chosen to be visualized (so called wave graph). The data from this line is then plotted for a certain instant as a function of the axial position. This kind of line plot is repeated for a series of successive instants (Figure 11).

It can be seen from the wave graph that from a qualitative point of view the wave velocity behind the obstacle is high close behind the obstacle and slowing down the further the waves propagate away from it.

4.2 Mean film thickness

The mean film thickness is calculated by averaging the film thickness at each point along one longitudinal line over the whole measurement duration. Figure 12 shows, that the water accumulates upstream of the obstacle. By the acceleration of the air under the obstacle the film thickness decreases until it passes the obstacle. Downstream of the obstacle the film thickness increases again. This is most probably due to the slowdown of the air flow.

It should be noted, that the second minimum at measuring point 40 is caused from a vortex in the air behind the obstacle. This vortex is visible during the experiments from the droplet motion at the side wall of the test channel.

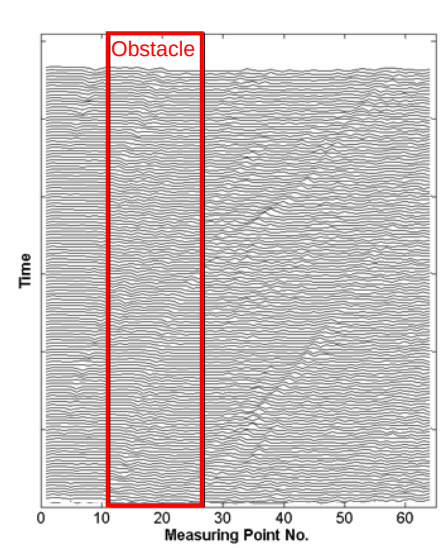

Fig. 11: Wave graph of measured data

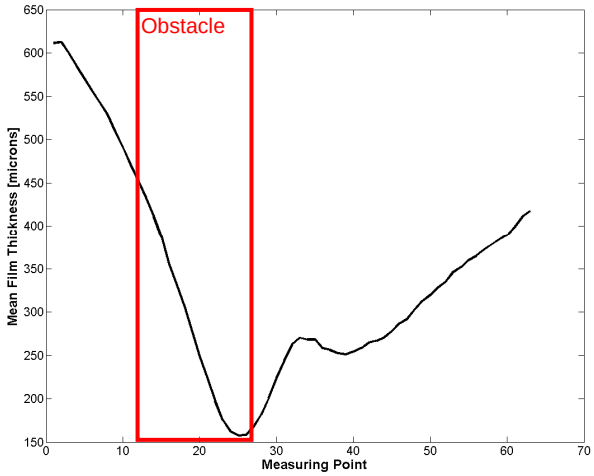

Fig. 12: Mean film thickness of one longitudinal line

4.3 Wave Analysis

As the surface wave properties of the liquid film are dependent on air and water velocity of the flow, the wave velocity, wavelength and wave frequency is from our point of view a distinct statistical property for the validation of CFD codes.

As it is know from literature, most wave patterns of high Re-number can be usually divided in ripple and disturbance waves (also called "roll waves"), which are propagating with different velocities. With the availability of high sampling frequency and good spatial resolution of our new sensor, we developed a method based on the continuous wavelet transform (CWT), to determine wave frequency resolved wave velocities.

The liquid film can be seen as a variety of waves consisting of different frequencies, velocities and lengths interfering with each other. These wave properties are time dependent. Hence a global view of the dynamic wave structure can only be achieved by a time and space resolved description of each wave. The CWT, as described below, is an elegant method for this kind of time resolved wave frequency analysis. It is based on Equation(1).

$$C(\tau,s)=\frac{1}{\sqrt{|s|}}\int x(t)\cdot\psi\left(\frac{t-\tau}{s}\right)dt \qquad (1)$$

From a practical point of view the CWT is similar to a cross correlation between the measured signal x and an artificial function ψ, the so called mother function.

This mother function has generally a mean of zero. In the analysis presented in this work, the mother function is a so called "Mexican hat" (Figure 13).

By scaling this function with the scale s, which is the reciprocal to the frequency, and integrating it over time, it filters the according frequency at the time τ. The received value is standardized by the reciprocal of the square rooted scale to receive the so called continuous wavelet transform coefficient C. For a deeper understanding of the wavelet transform the reader is referred to Farge (1992).

Compared to the (Short) Fast Fourier Transform the CWT has the advantage of receiving additional information of the occurrence time of the wave of a certain frequency, because the resolution of the occurrence time is adapted to the frequency of the analyzed wave. Further the wavelet transform allows filtering the signal with a shape that is closer to the shape of the wave than a sinus curve.

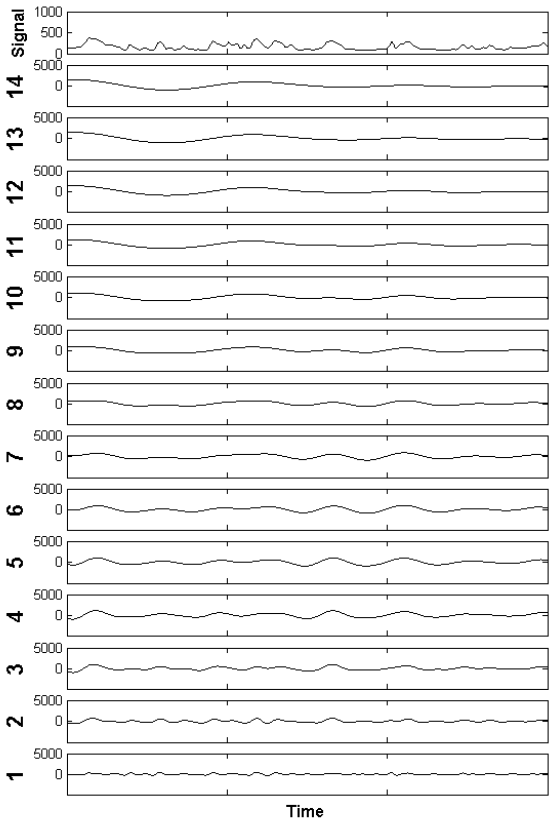

Fig. 14: CWT signal resolving for different scales in [ms]

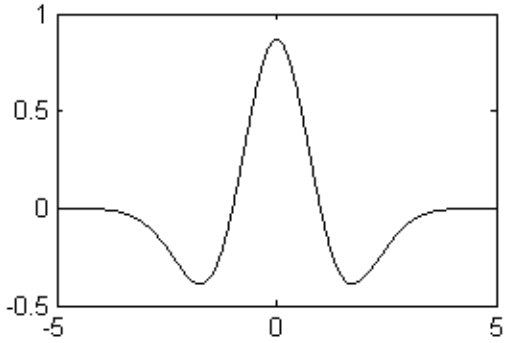

Fig. 13: Mexican hat function

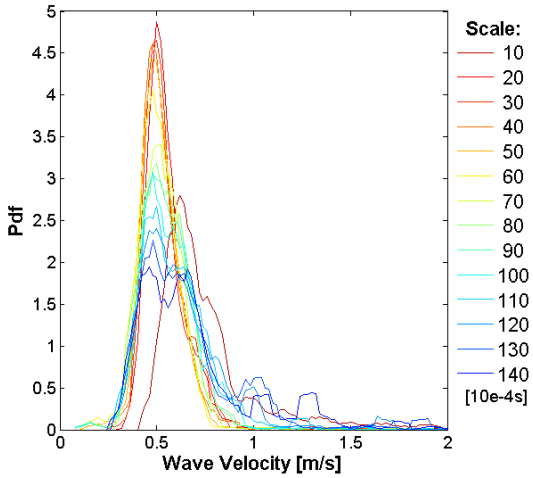

Fig. 15: PDF of wave velocities for different scales

The CWT presented in this work is carried out in the time domain, because the spatial resolution does not enable a precise analysis of the wavelength. Hence the wave frequency and wave velocity are calculated first. The wavelength can then be calculated with Equation (2).

$$c = \lambda \cdot f \tag{2}$$

The CWT in this work is used in its discretized form (Equation (3)):

$$C_{j,k} = \sqrt{\frac{\Delta t}{k}} \sum_i x_i \cdot \psi\left(\frac{i-j}{k}\right) \tag{3}$$

The time step Δt is 0.1ms corresponding to the maximum measurement frequency of the sensor. Figure 14 displays exemplary a time signal of one measuring point with the CWT coefficients C of different scales ranging from 1 to 14 ms (k=10, 20, 30,40,…140).
After the CWT of the experimental data received by the sensor, the cross correlation of the CWT coefficients of two consecutive measuring points C_m and C_{m+1} is calculated for each scale to receive the cross correlation values f of the signal at an instant l (Equation (4)).The wave velocities c are then calculated according to Equation (5) for different scales, instants and measuring points.

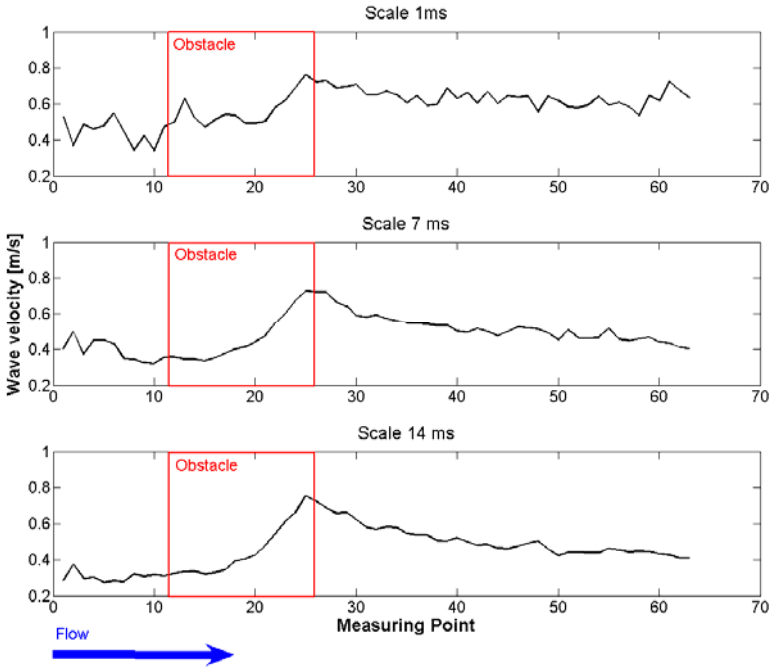

Fig. 16: Wave velocity for different scales: measured data (black) and simulation data (grey). No waves are existing upstream of point 30 due to stationary inlet conditions.

$$f_{l,j,k,m} = \frac{\sum_{i=l-5k}^{l+5k} C_{i,k,m+1} \cdot C_{i+j,k,m}}{\sqrt{\sum_{i=l-5k}^{l+5k} C^2{}_{i,k,m} \cdot \sum_{i=l-5k}^{l+5k} C^2{}_{i,k,m+1}}} \tag{4}$$

$$c_{l,k,m} = \frac{d}{\left(j\big|_{\max(f_{l,j,k,m})} - l \right) \bullet \Delta t} \tag{5}$$

For a stable solution of the time shift j with maximum f some boundary conditions had to be defined:

- The wave velocity is always in the direction of the gas flow (j > l).
- The range of the cross correlation is adapted to ten times the scale k of the wavelet transform to ensure that there is enough, but not too much signal available.
- To avoid the cross correlation of noise, the signal is only correlated, when the CWT coefficient at time l exceeds the mean absolute value of all CWT coefficients. Hence the velocity of the wave is analyzed from the extreme values of the waves.

The velocity is calculated for each scale on each measuring point along a center longitudinal line with a 5 ms time step (l=0, 50, 100,…) to keep calculation cost bearable. Figure 15 displays an example of the velocity distribution of one measuring point over the measuring time.

Figure 16 shows the results of the method described above applied to the measured data. From the measurement it can be seen, that small waves (1 ms scale) almost maintain their velocity over the whole length of the sensor. Waves with a scale of 7 ms speed up under the obstacle and slow down behind it. For bigger waves (14 ms scale) the same effect is seen.

5 CONCLUSION

A novel sensor based on the conductance method is presented that allows high-speed measurements of liquid film flows. This sensor has a time resolution of 10 kHz and 64x16 measuring points with a spatial resolution of 3.12 mm^2 and a maximum range of the film thickness of 0.8 mm.
Design principles are derived from the calculation of the potential field in the liquid film to optimize the electrode geometry. Various liquid films of known thickness have been imposed on top of the sensor to determine the sensor characteristic experimentally. The result is generally in good agreement with the calculated sensor characteristic. The sensor characteristic is further almost independent from the water conductivity and thus scalable by the saturation film thickness. Therefore the data of dynamic measurements is calibrated for each measuring point individually.

Visualization and statistical methods were used to characterize the film flow phenomena around an obstacle in a cross-sectional square channel. Among the statistical evaluation a new method based on the continuous wavelet transform (CWT) in combination with a cross-correlation has been applied, which takes advantage of the high time and good spatial resolution of the sensor. In this way scale-dependent wave velocities are calculated.
These methods were developed and tested on the experimental data and might be suitable to compare transient experiments and calculations, which by their chaotic or, respectively, stochastic nature cannot be compared directly in the time domain. Especially the wavelet analysis seems useful as a way of a "higher order" comparison that can be used to perform very sensitive checks of the performance of the theoretical models.

CFD validation with the data of the experiments described in this paper will be conducted with a URANS heterogeneous flow field model and LES. From the experience, which is being collected during preliminary simulation of the film flow so far, it becomes obvious, that the area around the interface has to be very well resolved to reach numerical stability. This implies that the time step has to be very small to satisfy the Courant criteria. Because of the need of transient simulations for the CFD validation, the simulation of annular flow has extremely high computational costs.

REFERENCES

Assad, A., et al., *Scaled entrainment measurements in ripple-annular flow in a small tube.* Nuclear Engineering and Design, 1998. **184**(2-3): p. 437-447.

Alekseenko, A., Guzanov, Kharlamov, and Markovich, *Evolution of solitary three-dimensional waves on vertically falling liquid films.* 6th International Conference on Multiphase Flow, Leipzig, Germany, 2007, 2007.

Belt R.J., V.t.W.J.M.C., Portela L.M., Mudde R.F., Oliemans R.V.A., Prasser H.-M., *Interfacial Waves and Shear-Stress in Vertical Upward Annular Pipe-Flow.* 6th International Conference on Multiphase Flow, ICMF2007, Leipzig, Germany, 2007.

Farge, M., *Wavelet Transforms and their Applications to Turbulence.* Annual Review of Fluid Mechanics, 1992. **24**(1): p. 395-458.

Kamei, T. and A. Serizawa, *Measurement of 2-dimensional local instantaneous liquid film thickness around simulated nuclear fuel rod by ultrasonic transmission technique.* Nuclear Engineering and Design, 1998. **184**(2-3): p. 349-362.

Prasser, H.M., A. Bottger, and J. Zschau, *A new electrode-mesh tomograph for gas-liquid flows.* Flow Measurement and Instrumentation, 1998. **9**(2): p. 111-119.

Sekoguchi, K., M. Takeishi, and T. Ishimatsu, *Interfacial structure in vertical upward annular flow.* PhysicoChemical Hydrodynamics, 1985. **6**(1/2): p. 239-255.

Takahama, H. and S. Kato, *Longitudinal flow characteristics of vertically falling liquid films without concurrent gas flow.* International Journal of Multiphase Flow, 1980. **6**(3): p. 203-215.